Oleylamine-mediated solvothermal synthesis of antimonene nanosheets

Sheng'en Qiu, Xiaoying Li and Zongping Chen*

State Key Laboratory of Silicon and Advanced Semiconductor Materials, School of Materials Science and Engineering, Zhejiang University, Hangzhou 310027, China

*E-mail: mailto:chenzp@zju.edu.cn

1. Experimental Section

1.1 materials

$SbCl_3$(99.99%), oleylamine (99.99%), antimony acetate (99.9%), potassium antimony tartrate (99.9%), Dimethyl Formamide (DMF, 99.99%) and ethanol (99.99%) were purchased from Macklin Co., Ltd. O-xylene (99.99%) were purchased from Aladdin Co., Ltd.

1.2 Characterization of the materials

Microstructural analysis was performed via transmission electron microscopy (TEM, JEOL JEM-F200) at an accelerating voltage of 200 kV. Phase coposition was examined by X-ray diffraction (XRD, Rigaku SmartLab SE) with Cu Kα radiation (λ = 0.154 nm), and chemical states were analyzed using X-ray photoelectron spectroscopy (XPS, Thermo Scientific K-Alpha) with monochromatic Al Kα excitation (1486.69 eV). Morphological characterization was performed using an Eclipse LV1000D optical microscope (Nikon). Thermogravimetric analysis (TGA) was conducted on a NETZSCH TG 209 system to quantify the adsorbed component content. Atomic force microscopy (AFM) measurements were carried out on a Cypher ES (Oxford Instruments).

2. Supplementary Figures

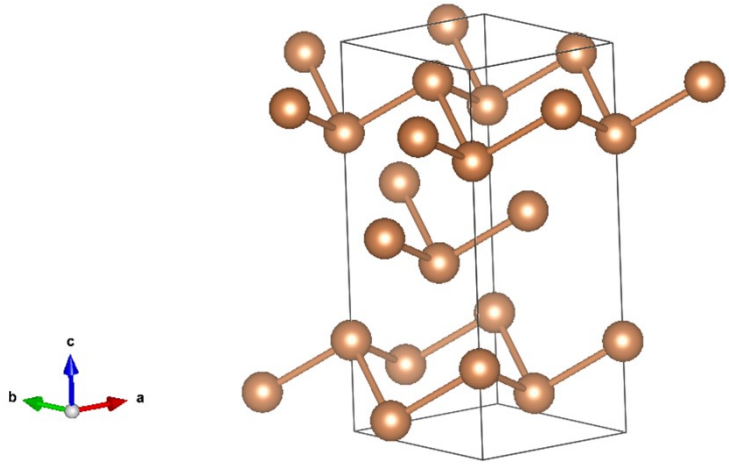

Figure S1. β-phase antimonene structure

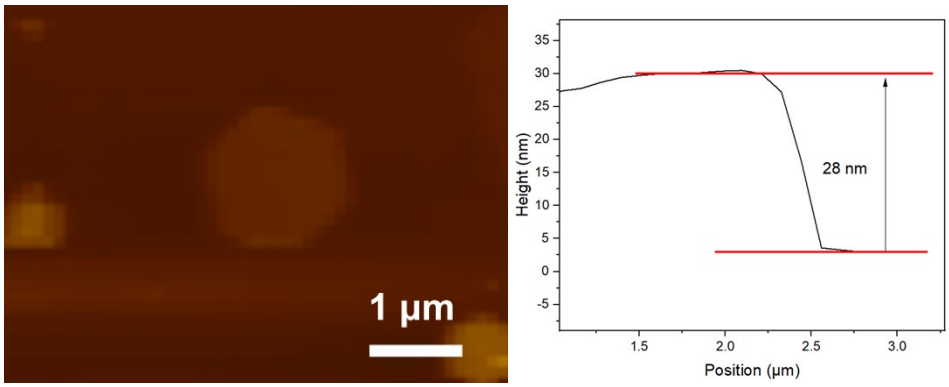

Figure S2. AFM image and height of antimonene nanosheet

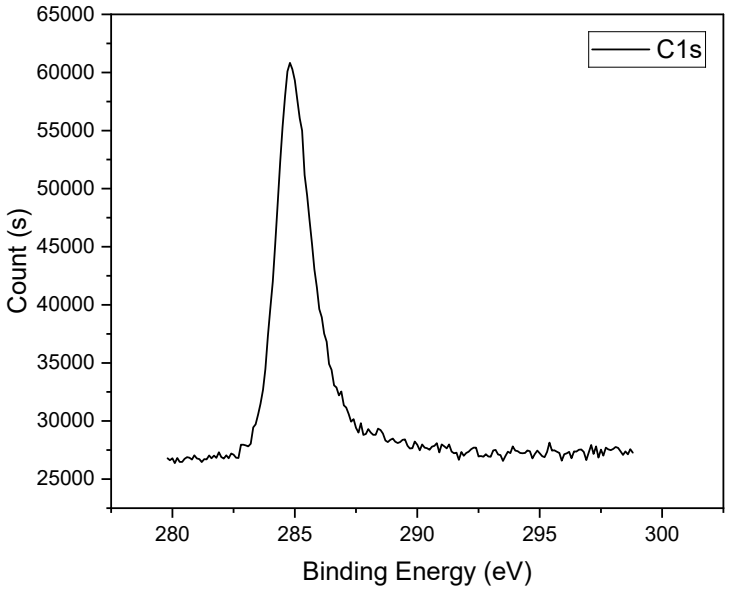

Figure S3. High-resolution XPS spectra for C elements.

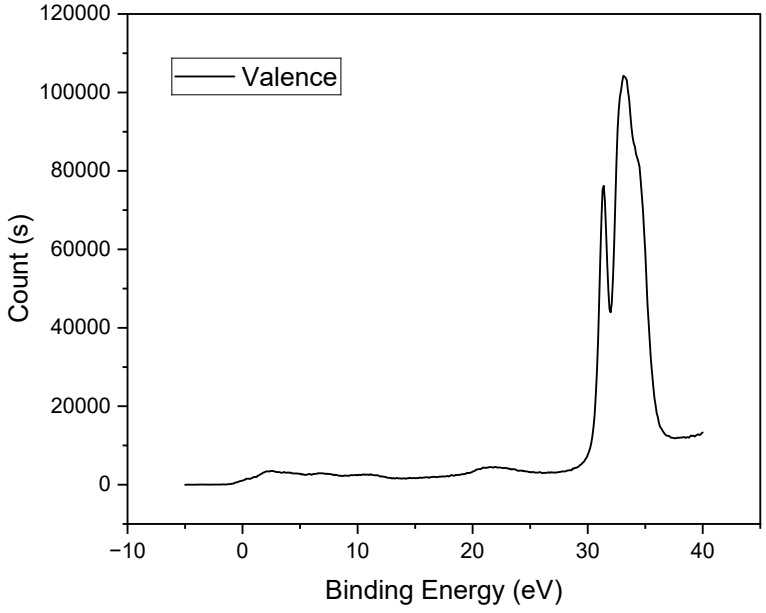

Figure S4. XPS valence band spectrum

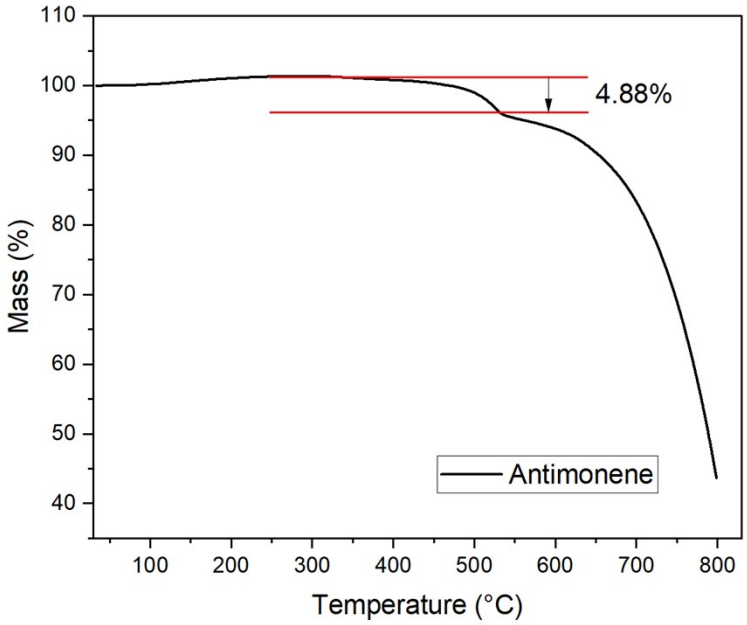

Figure S5. TGA curve of antimonene nanosheets.

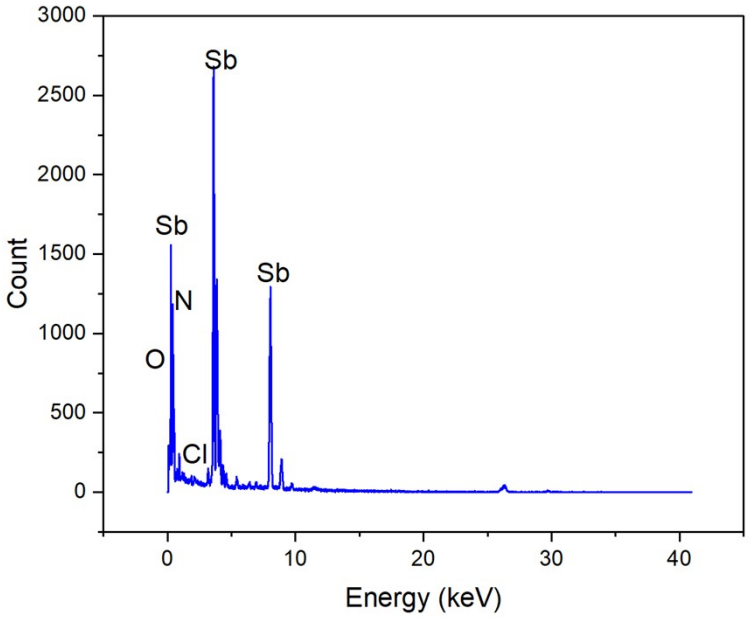

Figure S6. EDS spectrum of antimonene nanosheets.

Table S1 Quantitative analysis

Element	Mass (%)	Atom (%)	Sigma
Sb	94.35	67.04	0.91
Cl	0.10	0.25	0.03
N	3.51	21.69	0.12
O	2.04	11.02	0.09

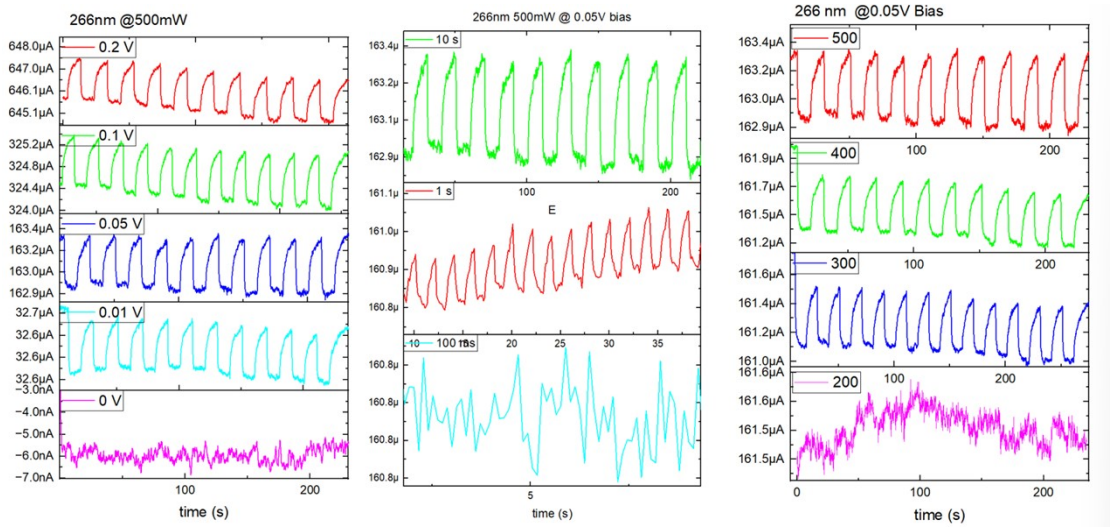

Figure S7. Photoresponse spectrum under 266 nm laser irradiation

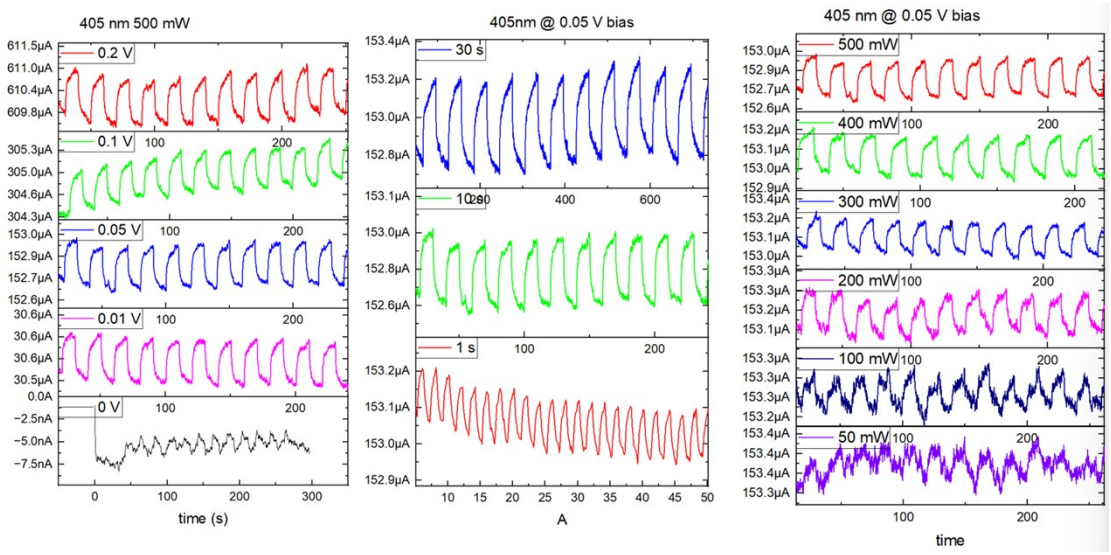

Figure S8. Photoresponse spectrum under 405 nm laser irradiation

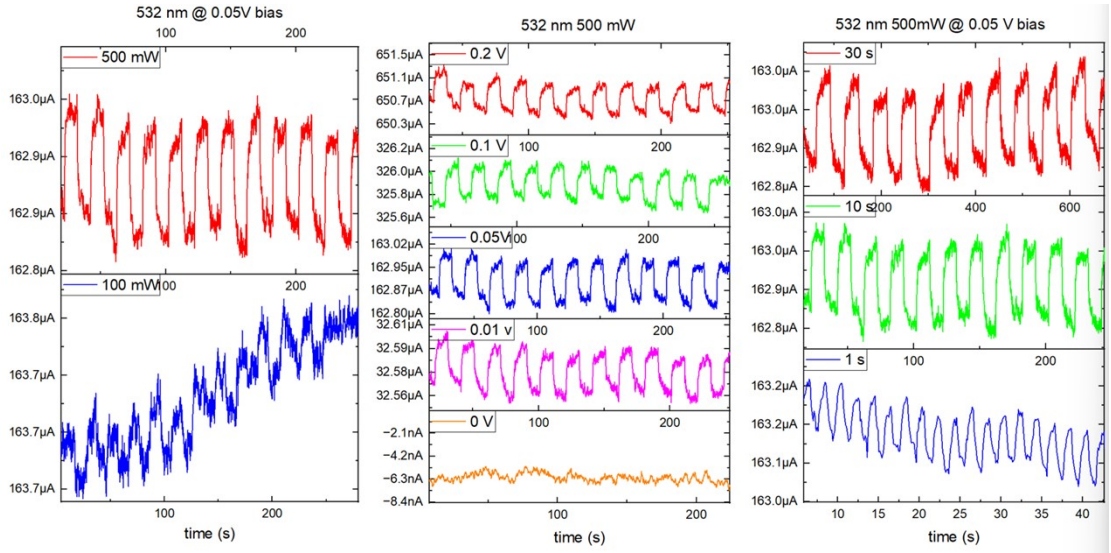

Figure S9. Photoresponse spectrum under 532 nm laser irradiation

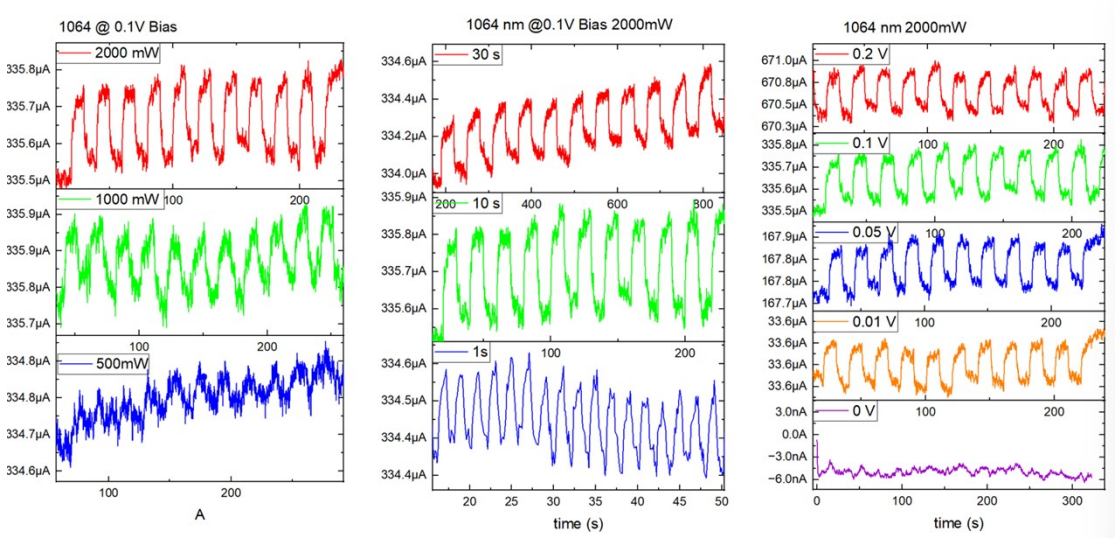

Figure S10. Photoresponse spectrum under 1064 nm laser irradiation

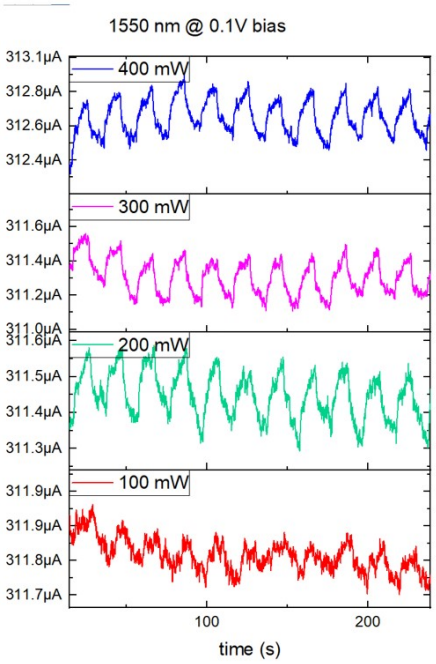

Figure S11. Photoresponse spectrum under 1550 nm laser irradiation

Table S2. Evolution of atomic concentrations for N, Cl element from in-situ XPS spectra

element	dark-I	irradiation	dark-II
N 1s	4.8	0.03	5.17
Cl 2p	22.99	0.04	22.63

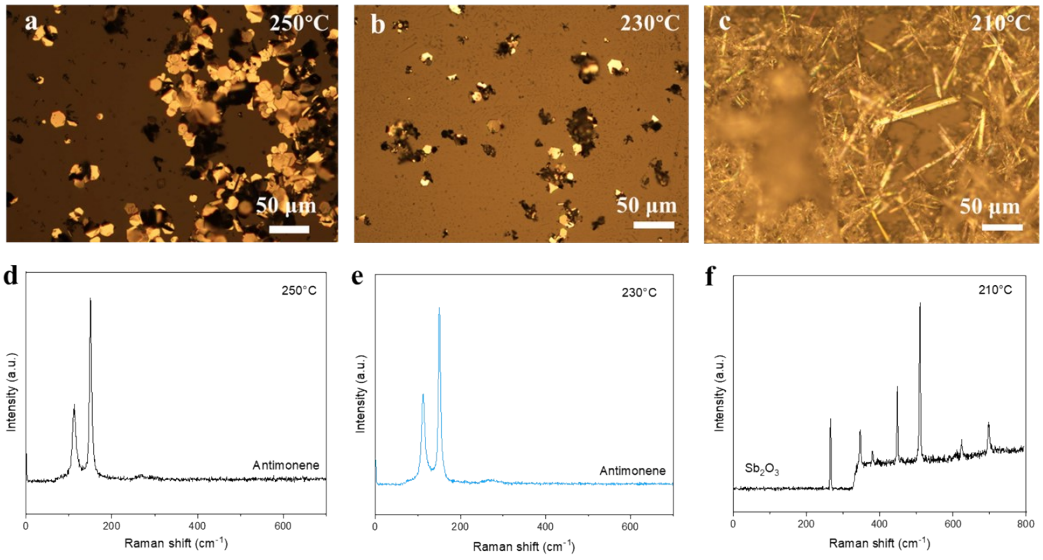

Figure S12. Optical micrographs and the corresponding Raman spectra of the products synthesized at different temperatures (250°C, 230°C, 210°C)

With decreasing temperature, the hexagonal morphology of the antimonene nanosheets is optimal at 250°C. At 230°C, the formation of non-hexagonal antimony bulk structures is observed alongside the nanosheets. A further decrease to 210°C results in the complete conversion of the product to antimony oxide.

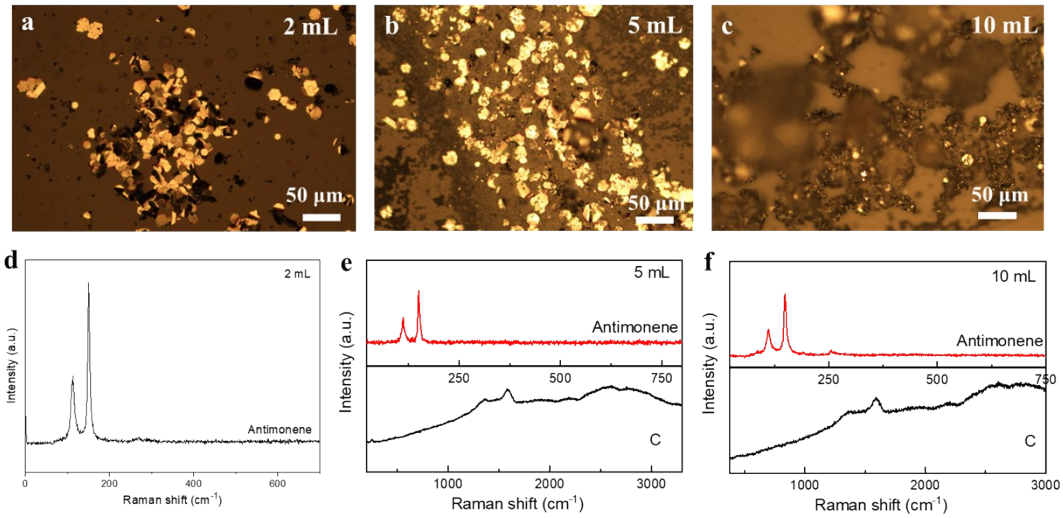

Figure S13. Optical micrographs and the corresponding Raman spectra of the products synthesized at different oleylamine concentration

As the oleylamine concentration increases, the carbon impurity in the products gradually rises. This is attributed to the excess oleylamine thermally decomposing and carbonizing under the high-temperature solvothermal conditions.

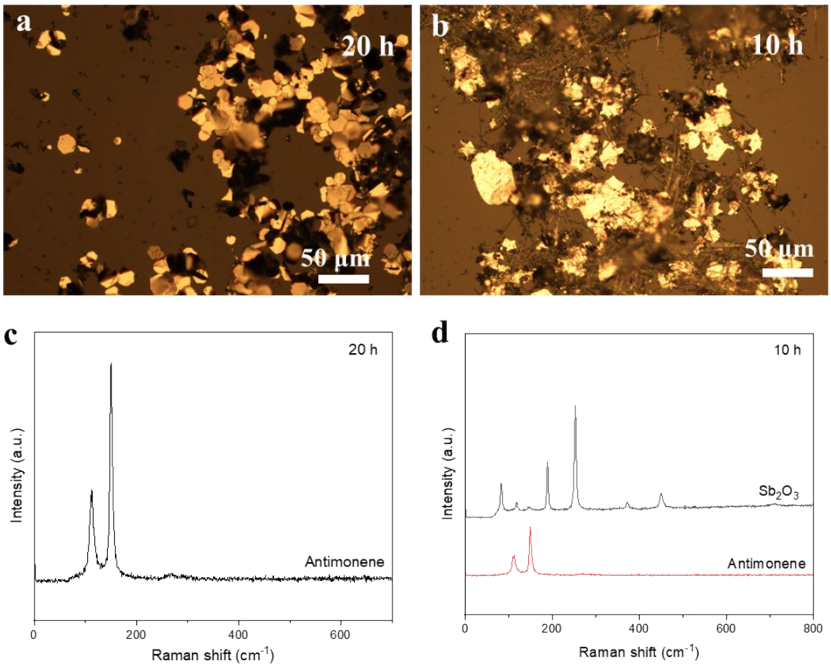

Figure S14. Optical micrographs and the corresponding Raman spectra of the products synthesized at different reaction time

When the reaction time was reduced to 10 hours, the emergence of Sb_2O_3 within the antimonene nanosheets was observed, which is attributed to an incomplete reaction.

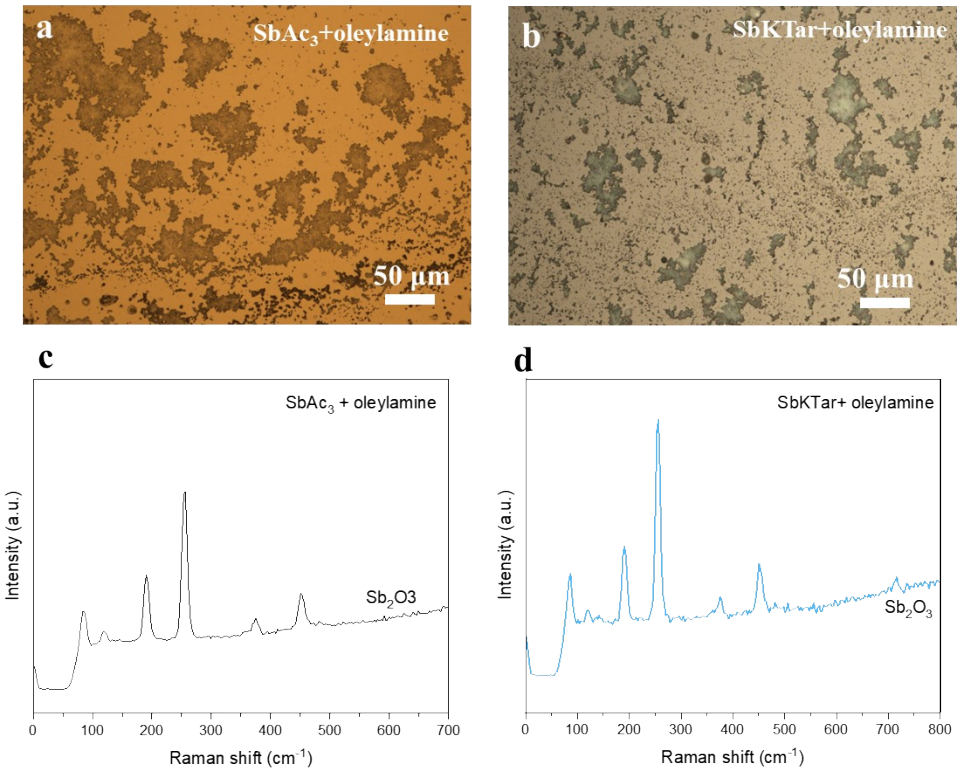

Figure S15. The morphology and Raman spectra of the products obtained from antimony acetate ($SbAc_3$) and potassium antimony tartrate (SbKTar) under the same solvothermal reaction conditions with oleylamine.

When $SbCl_3$ was replaced with $SbAc_3$ or SbKTar, the resulting products were identified as antimony oxide. This indicates that the presence of halogens plays a critical role in preventing oxidation during the reaction.